

## Article

# The Influence of Mountain Height and Distance on Shape Factor of Wind Load of Plastic Tunnel

Jing Xu  **1**, Xiaoying Ren **1**, Guifeng He **1**, Shaohan Di **2**, Zhiqing Shi **1** and Zongmin Liang **1,\***

**1** College of Water Conservancy and Civil Engineering, China Agricultural University, Beijing 100083, China; xujing@cau.edu.cn (J.X.); renxiaoxying@cau.edu.cn (X.R.); heguifeng@cau.edu.cn (G.H.); shizhiqing@cau.edu.cn (Z.S.)

**2** School of Civil Engineering, Beijing Jiaotong University, Beijing 100044, China; dishaohan@bjtu.edu.cn

\* Correspondence: sea9282@126.com

**Abstract:** Due to their soft structure and covering material, plastic greenhouses are vulnerable to wind disasters, causing large-scale damage and huge economic losses. The wind load of greenhouses depends on the surface wind pressure distribution, which is different for greenhouses located in valleys from those in plain areas. To study the wind pressure distribution law for various regions of greenhouses built in valleys, mountain and greenhouse models have been built by Computational Fluid Dynamics, in which the length direction of the greenhouse is perpendicular to the valley and the wind direction is parallel to the valley. In the analysis, the verified turbulence model and grid division method are both introduced, and the effect of the height and distance of mountains is considered. According to the distribution law of wind pressure, the greenhouse's surface is partitioned, and the variation law of the shape factor of wind load on a plastic tunnel is analyzed. Then, the calculation model for the shape factor of the wind load on the greenhouse located in a valley is proposed. The conclusions show that: (a) When the wind inflow direction angle is parallel to the valley, the distribution pattern of wind pressure on the surface of the greenhouse is similar to that on the plain regardless of the distance and height of the mountains, while the values of the wind pressure are greatly affected by the mountain height and distance. The distance between mountains has greater influence than the effect of mountain height. (b) The shape factor of wind load on the suction area of the greenhouse decreases as the distance of mountains increases, while the shape factor on the pressure area of the greenhouse increases with the increase in the distance. It can be seen that the valley effect is non-negligible. The narrower and deeper the valley, the greater the wind pressure effect. (c) When the ratio of the distance between the foot of the mountain and the greenhouse  $d$  to the height of the mountain  $H$  is less than 5, i.e.,  $d/H < 5$ , the ratio of the distance to the height has a significant impact on the shape factor of wind load on the greenhouse. When  $d/H$  is close to 10, the shape factor of the wind load in the valley area is close to that in the plain area, and the effect of the ratio between the height and the distance is negligible. (d) The proposed calculation model can be used to calculate the effect of mountain height and distance on the shape factor of wind load. The research results can be used in the wind resistance design of plastic greenhouses in valley areas, and can also provide some data support for the revision of the greenhouse structural load code.



**Citation:** Xu, J.; Ren, X.; He, G.; Di, S.; Shi, Z.; Liang, Z. The Influence of Mountain Height and Distance on Shape Factor of Wind Load of Plastic Tunnel. *Appl. Sci.* **2023**, *13*, 13081. <https://doi.org/10.3390/app132413081>

Academic Editor: Fabio Rizzo

Received: 6 November 2023

Revised: 3 December 2023

Accepted: 5 December 2023

Published: 7 December 2023



**Copyright:** © 2023 by the authors. Licensee MDPI, Basel, Switzerland. This article is an open access article distributed under the terms and conditions of the Creative Commons Attribution (CC BY) license (<https://creativecommons.org/licenses/by/4.0/>).

**Keywords:** valley; plastic greenhouse; shape factor of wind load; mountain height; computational model

## 1. Introduction

In recent years, more attention has been paid to the safety performance and structural design of flexible buildings [1,2]. As a typical flexible building, plastic greenhouses are an important agricultural infrastructure in China, whose development requires more attention. Currently, there are certain constraints affecting the construction of plastic greenhouses in Tibet. Firstly, most of the plastic tunnels in Tibet are built with reference to the structural

forms of plain areas, which lack local characteristics and geographical features and are difficult to adapt to the high-altitude and complex terrain of valleys. Secondly, plastic greenhouses are relatively lightweight and are highly susceptible to damage from wind and snow loads [3]. The wind load is related to wind pressure distribution. Tibet has high elevations and thin air, with air density in these areas different to that in plain areas. Influenced by valley airflow and mountainous terrain, the wind pressure distribution in Tibet differs from that in plain areas. Therefore, studying the wind pressure distribution characteristics of plastic tunnels in valley areas is of significant importance in the structural design of greenhouses to ensure their safety.

Wind load is one of the main loads to be controlled when designing engineering structures; many scholars have studied the characteristics of wind load under different working conditions [4–12], including studies on the influence of mountain topography, height and distance on wind load [13–18]. The shape factor of wind load is an indispensable parameter when calculating wind load, and it can be obtained by three methods: field tests [19–22], wind tunnel tests [23–26] and numerical simulations [26–41]. Wang et al. [19], Yang et al. [20] and Kwon et al. [22] obtained the wind pressure pattern using the wind tunnel test, while Li et al. [23] and Hoxey et al. [26] gained full-scale results for the wind pressure characteristic. In those studies, field tests and wind tunnel tests were relatively demanding on the structural dimensions and the environment. Numerical simulation is currently an essential approach to wind engineering, with the advantage of simulating real environmental and prototype dimensions, a short finish time and low costs [42]. Therefore, the CFD numerical simulation method is used to analyze the wind characteristics or wind pressure distribution. Yao et al. [31] and Zhang et al. [33] simulated the wind field characteristics in a valley terrain. Tao et al. [34], Lv et al. [35], Wu et al. [36], and Yan et al. [37] analyzed the wind pressure distribution on different types of greenhouses based on numerical simulation, but those studies are only suitable for greenhouses located on plain area. In general, fewer studies have been carried out on surface wind pressure patterns for greenhouses placed in valley areas.

In this study, to obtain the wind pressure distribution law and the shape factor of wind load on a single-span arched plastic tunnel laid in a valley region, mountain models and a greenhouse model have been built in the same wind flow field through CFD. The verified turbulence model and grid division method are applied in the analysis. The influence of the height of the mountain and distance between mountains on the distribution law of the wind pressure of the greenhouse is discussed. Then, based on the partition method, the shape factors of wind load on each surface area of the greenhouse are studied, and a calculation model for the shape factor of wind load is proposed. The research results can offer a supplement to the design of greenhouses in valley area.

## 2. Numerical Simulation Method

The wall function can directly correlate the uncertainty at the center of the turbulence area with the physical quantities on the wall, and modify the turbulence model by obtaining the values of the nodal variables in the control body. Compared to the Standard Wall Functions, which are more suitable for studying situations wherein the flow near the wall has little impact on the research object, Scalable Wall Functions can be flexibly adjusted according to the thickness of the near wall grid, and generate consistent results for any refined grids. As for our research object, the wind pressure distribution on the surface of the greenhouse is greatly affected by gas flow, and large differences arise between the sizes of the surface grid of the greenhouse and the grid sizes of the mountain. Scalable Wall Functions are chosen in this paper, as they are commonly used for studying fluid flow inside a model [43–45].

For both simple and complex flow fields, all fluid dynamics calculations must obey the conservation laws, including energy, mass, and momentum conservation laws, whose relevant expressions are all listed in Reference [46]. When the fluid is turbulent, an additional turbulence equation needs to be added.

This study evaluates the quality of different turbulence simulations by selecting six different turbulence models for numerical simulation, based on a simple cubic three-dimensional model, and comparing them with the wind tunnel tests conducted by Murakami [47] and the results measured on-site by Richard [48], in order to provide a basis for the subsequent simulation analysis. Figure 1 shows the wind pressure distributions calculated by the six different turbulence models at the center of the cube, and compares the simulation results with the results of wind tunnel tests and field tests. Finally, the Realizable  $k - \varepsilon$  model is chosen, which can more effectively match the wind tunnel test and measured results, whether on the simulated windward surface or at the simulated maximum negative pressure [38,39]. The main expression of the Realizable  $k - \varepsilon$  model is as follows:

$$\frac{\partial(\rho k)}{\partial t} + \frac{\partial(pku_i)}{\partial x_i} = \frac{\partial}{\partial x_j} \left[ \left( \mu + \frac{u_t}{\sigma_k} \right) \frac{\partial k}{\partial x_j} \right] + G_k - p\varepsilon \quad (1)$$

$$\frac{\partial(\rho\varepsilon)}{\partial t} + \frac{\partial(p\varepsilon u_i)}{\partial x_i} = \frac{\partial}{\partial x_j} \left[ \left( \mu + \frac{u_i}{\sigma_g} \right) \frac{\partial \varepsilon}{\partial x_j} \right] + C_2 p \frac{\varepsilon^2}{k + \sqrt{v\varepsilon}} \quad (2)$$

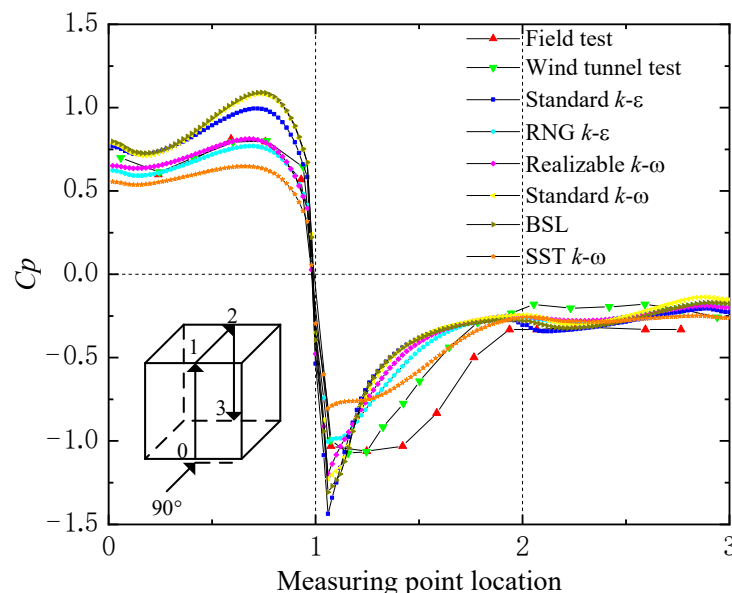


**Figure 1.** Distribution curves of wind pressure coefficients for different turbulence models.

In Equations (1) and (2),  $\rho$  is the fluid density;  $k$  is the turbulence kinetic energy, whose expression can be found in Reference [39];  $\varepsilon$  is the turbulence dissipation ratio, whose expression can be found in Reference [39];  $p$  represents the energy transport term;  $t$  represents time;  $u_i, u_t$  represent the velocity vector;  $x_i, x_j$  are the coordinate value;  $\mu$  represents the dynamic viscosity;  $\sigma_k, \sigma_g$  are the model constants;  $G_k$  represents the generation of turbulent kinetic energy caused by the average velocity gradient;  $C_2$  is the constant value and equals 1.9;  $v$  represents velocity.

### 3. Model Parameters

The most widely used form of arch-shaped plastic greenhouse in China is simulated, with the dimensions of length ( $L$ )  $\times$  span ( $S$ )  $\times$  height ( $H_G$ )  $\times$  shoulder height ( $H_L$ ) = 44 m  $\times$  7 m  $\times$  3.5 m  $\times$  1.6 m, and with a rise–span ratio of 0.27, as shown in Figure 2.

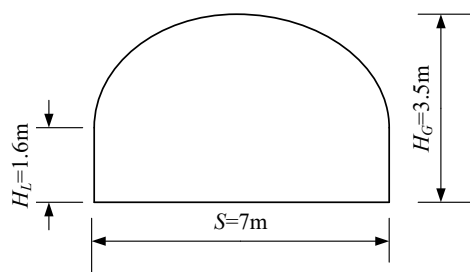


**Figure 2.** Dimensions of plastic greenhouse.

To improve the computational efficiency, the sine model of the undulating terrain  $H_1[1 + \cos(\pi r/2L_1)]/2$  is selected as the contour equation  $Z(x)$  of the mountain in the study of the wind load characteristics of a typical valley area. The parameter of the contour equation is shown in Figure 3a, and the layout of the mountains and greenhouse is shown in Figure 3b.

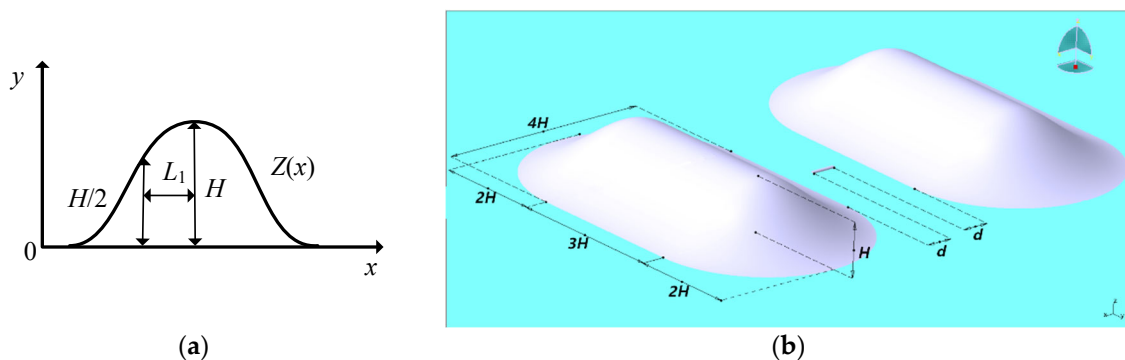


**Figure 3.** Skeleton map of mountain model and layout of mountains and plastic greenhouse.  
(a) Contour equation parameter of Sine model; (b) layout of mountains and greenhouse.

As shown in Figure 3,  $H$  is the mountain height, which is given values of 200 m, 400 m and 600 m in the simulation.  $L_1$  is the horizontal distance from the peak point  $H_1$  to the halfway point of the mountain  $H/2$ . The diameter of the mountain model is  $4H$ , the length of the ridge is  $3H$ , and the slope of the mountain is fixed at 0.5. We locate the greenhouse in the middle of the two mountains.  $d$  is the horizontal distance between the greenhouse and the bottom of the mountain.

#### 4. Model Partition and Simulation Analysis

##### 4.1. Model Partition of Greenhouse

The mountain and greenhouse models are established using the propriety modeling module. The verified grid division method [39] is used to partition the windward side, leeward side, crosswind sides and the roof of the greenhouse, as shown in Figure 4. According to the size of the plastic greenhouse and the height of the mountain,  $6H$  is taken from upstream and both sides of the flow field,  $7H$  is taken from the height direction, and  $15H$  is taken from the downstream area of the flow field, where  $H$  is the height of the mountain. The model is placed in the front 1/3 of the wind field calculation domain, and the model blocking rate is set at less than 3% to reduce the fluid's interaction with the boundary [46]. This article sets the surface grid size of the greenhouse to 0.1 m, the mountain surface grid size to 6.667 m, and the generated surface grid number to about 100,000, as shown in the Figure 5a. The maximum size of the volume grid is set to 50 m, and the number of generated volume grids ranges from 1.2 million to 2 million. The greenhouse, mountain, and bottom boundary layers are set to six layers, as shown in Figure 5b. The conversion rate is set to 0.1, and the growth rate is set to 1.1.

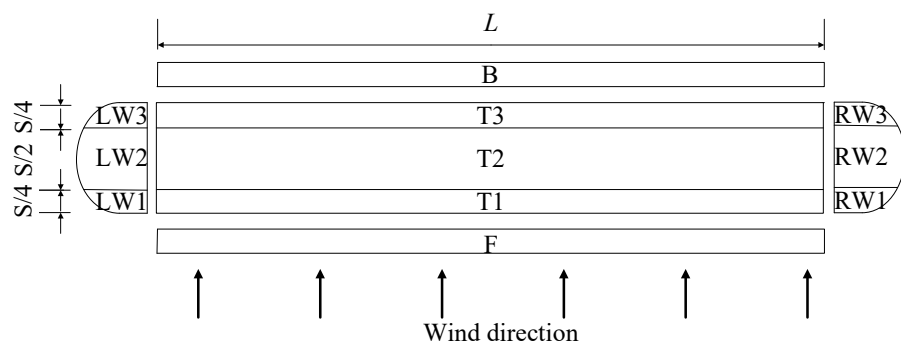


**Figure 4.** Wind direction and zoning diagram of wind pressure distribution on a plastic greenhouse.

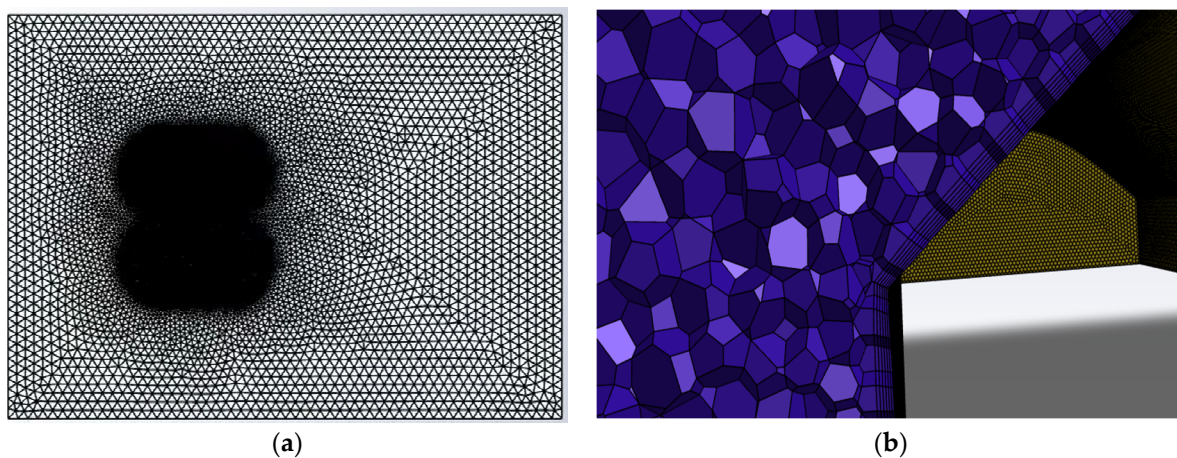


**Figure 5.** Schematic diagram of surface grid and boundary layer division. (a) Global schematic diagram of surface mesh division; (b) wall boundary layer mesh.

In this section, the azimuth angle of the greenhouse is fixed at  $0^\circ$  to analyze the influence of mountain heights  $H$  and distances  $d$  on the wind pressure distribution on the greenhouse. In Figure 4,  $L$  is the longitudinal span of the greenhouse;  $F$  and  $B$  represent the windward side and leeward sides of the plastic greenhouse, respectively.  $T1$ ,  $T2$  and  $T3$  are the three areas of the roof, respectively, while  $LW1$ ,  $LW2$  and  $LW3$  represent the left gable area, and  $RW1$ ,  $RW2$  and  $RW3$  represent the right gable area.

#### 4.2. Formula for the Shape Factor of Wind Load

The wind pressure coefficient is an important index used to analyze the surface pressure on a building. According to Bernoulli's principle, the wind pressure coefficient can be defined as the ratio of the net wind pressure at any measuring point on the surface of the building to the average dynamic pressure of the upstream incoming wind at the front-most surface of the building, whose expression is shown in Reference [39]. The shape factor of wind load is the area-weighted value of the wind pressure coefficient, as shown in Reference [39].

To better compare the shape factor of wind load on greenhouses located in valleys with those in plain areas, the correction factor for the shape factor of wind load in the valley is introduced as follows:

$$\eta = \frac{\mu_s}{\mu_{sv}} \quad (3)$$

In Equation (3),  $\mu_{sv}$  is the shape factor of wind load in the plain area;  $\mu_s$  is the shape factor of greenhouses in valley areas.

#### 4.3. Simulation Results and Analysis with Different Mountain Heights

In this section, the influence of mountain height on the shape factor of wind load is investigated. Different working conditions of mountain distance  $d$  are also considered. Then, the simulation results are illustrated and analyzed.

##### 4.3.1. Results and Analysis with a 200 m Mountain Height

The influence of a 200 m mountain height on the shape factor of wind load on plastic greenhouses is studied, with eight working conditions of the mountain distance  $d$  selected in the analysis. The nephograms of wind pressure distribution on the surface of the greenhouse and the values of the shape factor of wind load are shown in Figures 6 and 7, respectively. The correction factor of the shape factor is shown in Figure 8.

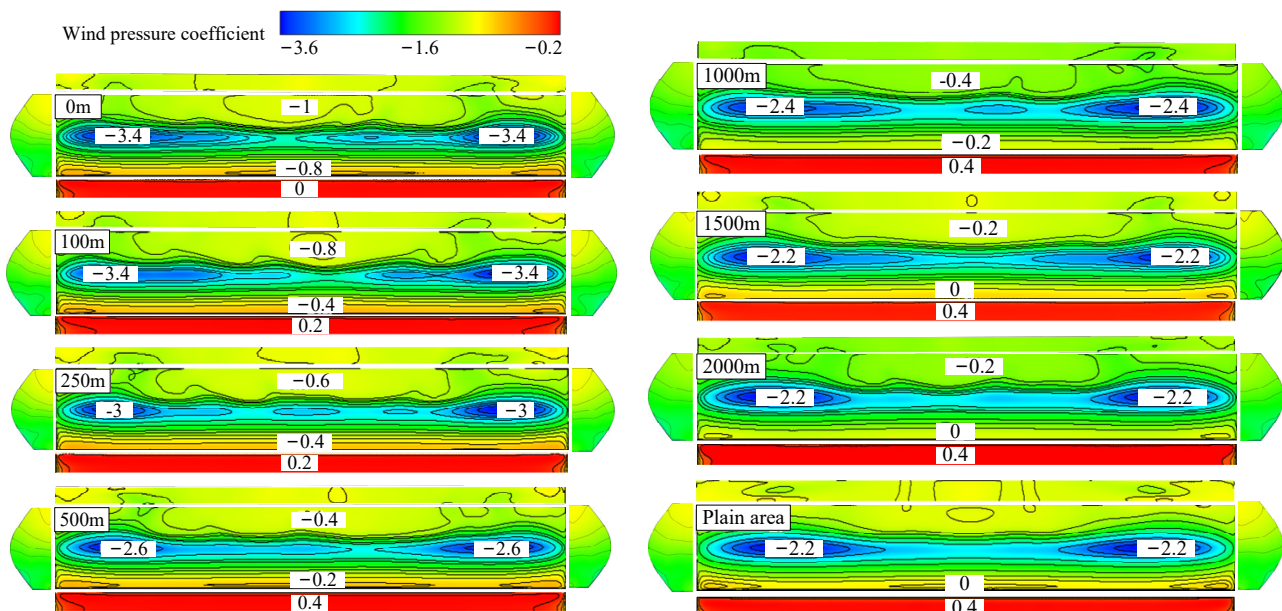


**Figure 6.** Wind pressure distribution on greenhouse with 200 m mountain height.

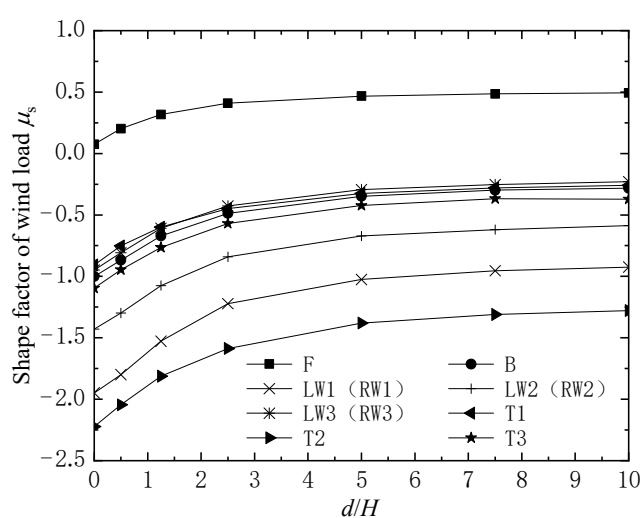


**Figure 7.** Shape factor of wind load with 200 m mountain height.

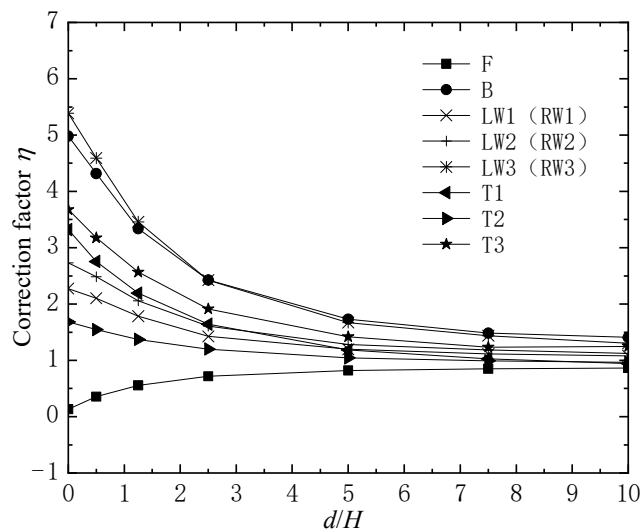


**Figure 8.** Correction factor for shape factor of wind load with 200 m mountain height.

It can be seen from Figure 6 that the surface wind pressure distribution law on a greenhouse in a valley is the same with that in a plain area. With the increase in the distance between the greenhouse and the mountain, the positive pressure on the greenhouse increases and the wind suction decreases.

In terms of the curve steepness, Figures 7 and 8 show that when the mountain height is 200 m, the shape factor of wind load and its correction factor undergo a noticeable change, with  $d/H < 5$ , which requires special attention in the design. Then, flat curves occur, and the values of the shape factor in the valley area approach those on plain terrain, with  $d/H > 5$ .

Figures 7 and 8 also show that for the windward area F, the further the mountain is from the greenhouse, the greater the surface wind pressure coefficient on the greenhouse, and the corresponding correction factor on the windward area F is less than 1.0 and gradually increases with the increasing of  $d/H$ , which indicates that a narrower valley has a weakening effect on the positive pressure of the windward area F.

For other areas, suction occurs, regardless of how the distance between the greenhouse and the mountain varies. The correction factors are all greater than 1.0, which means a narrower valley enlarges the effect of wind suction load on greenhouse. For the crosswind area, the absolute values of the shape factor for area LW1/RW1 are the biggest, followed by area LW2/RW2, and area LW3/RW3, while the correction factor for the area LW3/RW3 is the biggest, followed by LW2/RW2 and area LW1/RW1. This means that area LW3/RW3 is the most affected by the valley effect. For the roof area, the absolute values on area T2 are significantly greater than those on area T3 and T1, while the correction factor on area T3 is the biggest, which means area T3 is the most affected by the valley.

#### 4.3.2. Results and Analysis with 400 m Mountain Height

The influence of a 400 m-high mountain on the surface wind pressure distribution of the greenhouse is simulated, and the ten working conditions of mountain distances  $d$  of 0 m, 250 m, 500 m, 1000 m, 2000 m, 2500 m, 3000 m, 3500 m and 4000 m and the plain area are chosen for analysis. The nephogram of wind pressure distribution on the greenhouse and the value of the shape factor of the wind load are shown in Figures 9 and 10, respectively. The correction factor for the shape factor of wind load is shown in Figure 11.

Comparing Figure 9 with Figure 6, we see that the surface wind pressure distribution law is consistent. When distance  $d$  is equal to 0 m, negative pressure occurs on the windward side F. This suggests that when the mountain height is large enough, there may be negative pressure on the windward side F. With the increase in the distance  $d$ , the pressure on area F changes from negative to positive, and gradually approaches the value in the plain area.

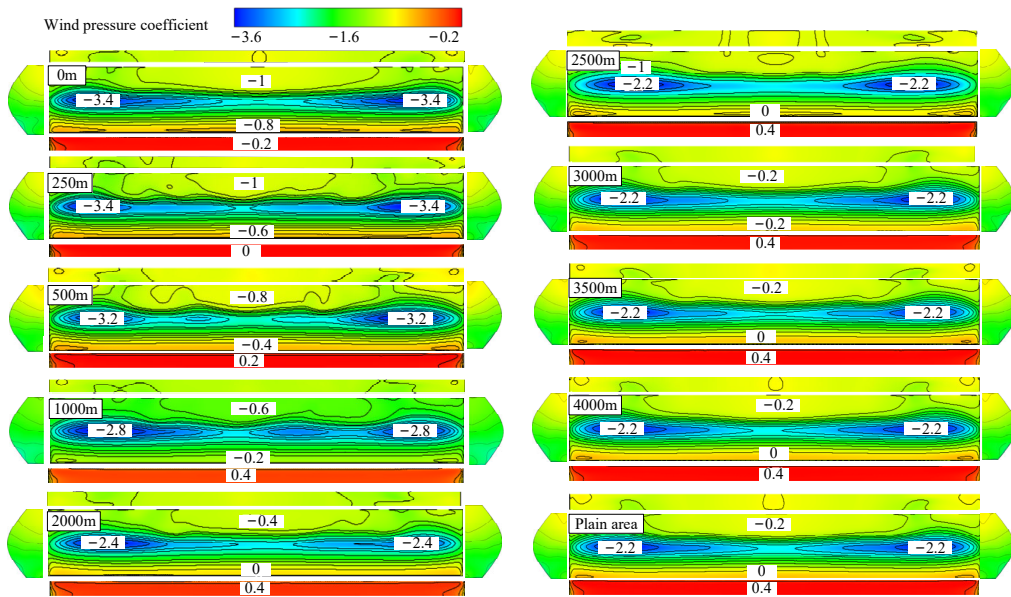


**Figure 9.** Wind pressure distribution of greenhouse with 400 m mountain height.

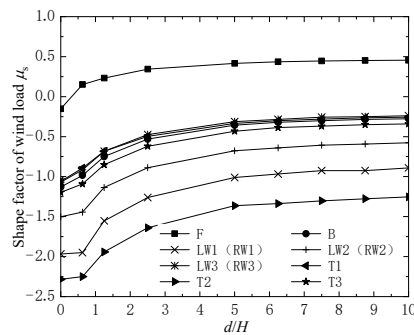


**Figure 10.** Shape factor of wind load with 400 m mountain height.

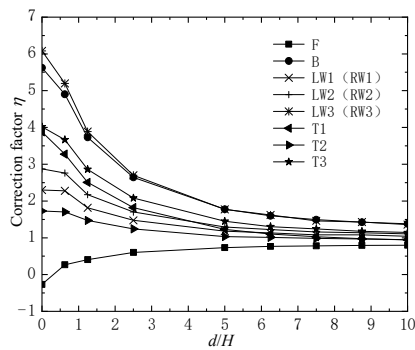


**Figure 11.** Correction factor for shape factor of wind load with 400 m mountain height.

From Figures 10 and 11, it can be inferred that suction is consistently applied on all other areas, which is consistent with the above results. The curve variation trend and the numerical variation trend of shape factors and correction factors on each area are consistent with Figures 7 and 8. When  $d/H < 5$ , the curve changes sharply, and when  $5 < d/H < 10$ , the valley has little significant influence on shape factors and their correction factors for all areas of the greenhouse.

#### 4.3.3. Results and Analysis with 600 m Mountain Height

The influence of a 600 m-high mountain on the wind pressure distribution is studied, and the eleven working conditions of mountain distances  $d$  of 0 m, 500 m, 1000 m, 1500 m,

2000 m, 2500 m, 3000 m, 3500 m, 4000 m, 5000 m and 6000 m and the plain area are applied. The nephogram of wind pressure distribution and the values of the shape factor of the wind load are shown in Figures 12 and 13, respectively, and the correction coefficient for the shape factor of the wind load is shown in Figure 14.

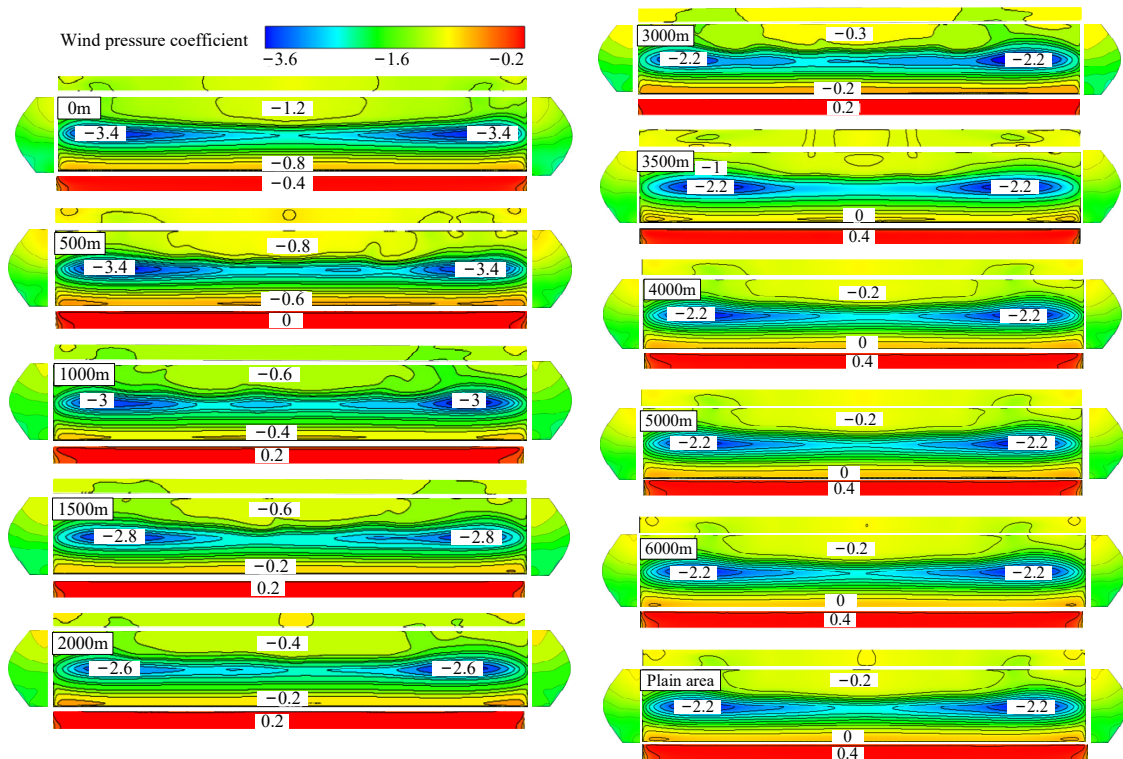


**Figure 12.** Wind pressure distribution of greenhouse with 600 m mountain height.

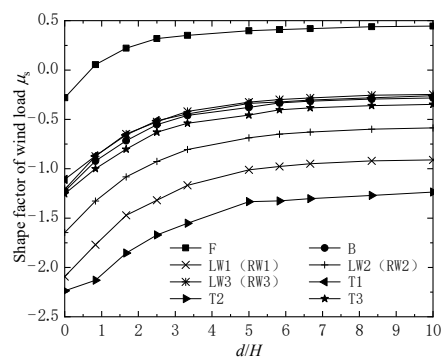


**Figure 13.** Shape factor of wind load with 600 m mountain height.

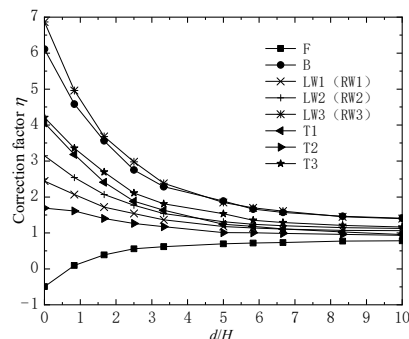


**Figure 14.** Correction factor of shape factor of wind load with 600 m mountain height.

Comparing Figure 12 with Figures 6 and 9, we see that the surface wind pressure distribution law remains consistent. When the distance  $d$  is equal to 0 m, the absolute value of negative pressure on the windward side F becomes bigger. This proves the above prediction that with the increasing in mountain height, the negative pressure load will increase. When the distance  $d$  increases to a certain value, the pressure on area F changes from negative to positive, and gradually approaches the value in the plain area.

As shown in Figures 7, 10 and 13, suction is consistently applied on each area except for area F, which adheres with the above conclusions. From Figures 8, 11 and 14, it is obvious that for each of these areas, the correction factors increase with the increase in mountain height. When  $d/H < 5$ , the curve changes sharply, and when  $5 < d/H < 10$ , the valley effect has an insignificant influence on shape factors and corresponding correction factors.

#### 4.3.4. Comparison and Analysis of Simulation Results with Different Mountain Heights

The shape factors of wind load as influenced by different mountain heights shown in Figures 7, 10 and 13 are summarized and compared in Figure 15. It can be seen from Figure 15 that for the same greenhouse area, the change in the shape factor of wind load is limited by the different mountain heights. The shape factor of wind load is mainly affected by the value of  $d/H$ : when  $d/H$  is less than 5, the shape factor of the wind load changes greatly. When  $5 < d/H < 10$ , the curve is relatively smooth, and the simulation results for the valley area are close to those for the plain terrain. When the mountain height is the same, the shape factors of wind load on different areas of the greenhouse are also quite different.

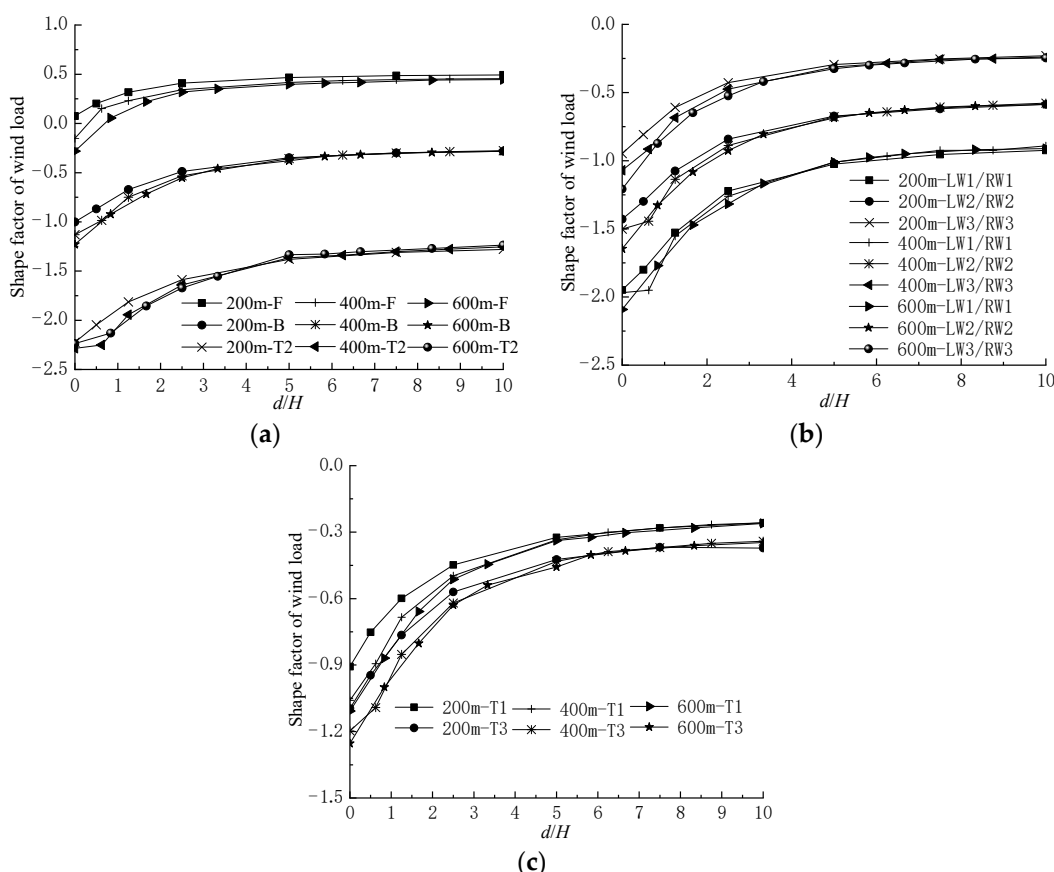


**Figure 15.** Comparison of shape factors of wind load with different mountain heights. (a) Windward side F, leeward side B and roof side T2; (b) crosswind side; (c) roof side T1 and T3.

#### 4.4. Calculation Model for Shape Factor of Wind Load

To simplify the calculation model, considering that mountain height has relatively little influence on the shape factor of the wind load, the ratio of distance  $d$  to mountain

height  $H$  is applied. After this, a curve is fitted to the relationship between the shape factor of the wind load  $\mu_s$  and  $d/H$ , as shown in Figure 15. The relationship curve was fitted using the calculation model developed by a previous research group [39], and the formula of the calculation model is as follows:

$$\mu_s = A - C \times D^Y \quad (4)$$

In Equation (4),  $A$ ,  $C$ , and  $D$  are the values of the fitting coefficient, and  $Y$  represents  $d/H$ . The fitting coefficient and correlation coefficient of the calculation model for different areas of the greenhouse are shown in Table 1.

**Table 1.** The fitting coefficients of the model in each area of the greenhouse.

Coefficient	F	B	LW1/RW1	LW2/RW2	LW3/RW3	T1	T2	T3
$A$	0.495	-0.271	-0.887	-0.570	-0.236	-0.245	-1.217	-0.329
$C$	0.419	0.957	1.205	1.076	0.972	0.863	1.020	0.925
$D$	0.585	0.646	0.675	0.661	0.632	0.670	0.672	0.676
Correlation coefficient $R^2$	0.973	0.995	0.993	0.996	0.995	0.992	0.941	0.993

Table 1 shows that all the correlation coefficient  $R^2$  values are greater than 0.9, which means the results derived from the calculation model are in good agreement with those of the numerical simulation. The proposed model can be applied to calculate the shape factor of the wind load of a plastic tunnel located in a valley area.

## 5. Conclusions

In this paper, three models featuring different mountain heights have established by numerical simulation to analyze the influence of mountain height and mountain distance on wind pressure distribution and the shape factor of the wind load on the surface of a greenhouse. The sine model was chosen as the contour equation of the mountain model. Therefore, the conclusions are mainly applicable to the mountain in the form of a sine curve. The main conclusions are as follows:

(a) When the inflow direction is parallel to the mountain valley, regardless of the distance between the mountains and the height of the mountain, the distribution law of wind pressure on the surface of the greenhouse located in a valley is similar to that for a greenhouse on a plain area, and only the values of positive/negative pressure coefficients are different;

(b) When the greenhouses are located in valley areas with different mountain heights, the valley will have a greater influence on the shape factor of the wind load on areas LW3/RW3, B, T1 and T3 of the greenhouse. The mountain will weaken the positive pressure on the windward side, which is beneficial to the windward area F. The suction on each surface of the greenhouse decreases with the increase in the distance  $d$  between the greenhouse and the mountain, while the shape factor of the wind load on each pressure area increases with the increase in the distance  $d$ ;

(c) When the ratio of the distance  $d$  to the height of the mountain  $H$  is less than 5, that is,  $d/H < 5$ , the mountain will have a large influence on the shape factor of the wind load of the greenhouse. When  $d/H > 10$ , the influence of the mountain's height on the shape factor of wind load will be negligible;

(d) A computational model for deriving the shape factor of the wind load is here proposed, and this can be used to calculate the wind load acting on the surface of a greenhouse in a valley area, and it can also provide data support for the revision of load codes regarding the design of greenhouse structures.

**Author Contributions:** Conceptualization, J.X. and Z.L.; software, G.H. and X.R.; data curation, Z.S. and J.X.; writing—original draft preparation, X.R. and S.D.; writing—review and editing, J.X.; visualization, G.H. and J.X. All authors have read and agreed to the published version of the manuscript.

**Funding:** This research work was supported by the National Natural Science Foundation of China (U20A2020), Beijing Innovation Consortium of Agriculture Research System (BAIC01-2023-20) and Ministry of Education of the People's Republic of China (C21JB0100060).

**Institutional Review Board Statement:** Not applicable.

**Informed Consent Statement:** Not applicable.

**Data Availability Statement:** The data presented in this study are available in article.

**Conflicts of Interest:** The authors declare that they have no known competing financial interests or personal relationships that could have appeared to influence the work reported in this paper.

## References

- Wei, H.; Chen, K.; Yan, Y. Design wind loads for local flexible cladding of structures based on wind tunnel tests. *J. Build. Eng.* **2021**, *44*, 103154.
- Huang, H.; Li, X.; Xue, S.; Luo, Y.; Shi, D.; Hou, X.; Liu, Y.; Li, N. Performance and Measurement Devices for Membrane Buildings in Civil Engineering: A Review. *Appl. Sci.* **2022**, *12*, 8648. [[CrossRef](#)]
- Min, Z.; Sun, G.; Chen, H. Development prospect and countermeasures of facility agriculture in Tibet. *Tibet. J. Agric. Sci.* **2006**, *28*, 42–48.
- Zou, Y.F.; Fu, Z.Y.; He, X.H.; Jing, H.Q.; Li, L.Y.; Niu, H.W.; Chen, Z.Q. Characteristics of wind loading on internal surface and its effect on wind-induced responses of a super-large natural-draught cooling tower. *Wind. Struct.* **2019**, *29*, 235–246.
- Tao, W.; Lou, P.; Zou, Y.; Cai, C.; He, X.; Jiang, S. Effects of Curved Wind Barrier on the Aerodynamic Characteristics of a Train-Bridge System and Its Static Wind Load. *Int. J. Struct. Stab. Dyn.* **2022**, *22*, 2241006. [[CrossRef](#)]
- Tang, L.; Liu, H.; Zheng, C. Effects of twisted wind flow on the mean wind load characteristics of super high-rise buildings with different heights. *J. Build. Eng.* **2023**, *75*, 106972. [[CrossRef](#)]
- Liu, Z.; Zheng, C.; Wu, Y.; Flay, R.G.; Zhang, K. Investigation on the effects of twisted wind flow on the wind loads on a square section megatall building. *J. Wind. Eng. Ind. Aerodyn.* **2019**, *191*, 127–142. [[CrossRef](#)]
- Fu, J.Y.; Li, Q.S.; Wu, J.R.; Ni, Z.H.; Xie, Z.N.; Gu, M. Spectral Characteristics and Correlation of Dynamic Wind Loads of a Typical Super-tall Building. *Struct. Design Tall Spec. Build.* **2008**, *17*, 471–489. [[CrossRef](#)]
- Li, Y.G.; Liu, P.; Li, Y.; Yan, J.H.; Quan, J. Wind loads characteristics of irregular shaped high-rise buildings. *Adv. Struct. Eng.* **2023**, *26*, 3–16. [[CrossRef](#)]
- Uematsu, Y.; Stathopoulos, T.; Iizumi, E. Wind loads on free-standing canopy roofs: Part 2 overall wind forces. *J. Wind. Eng. Ind. Aerodyn.* **2008**, *96*, 1029–1042. [[CrossRef](#)]
- Fu, J.; Li, Q.; Xie, Z. Wind effects on a large cantilevered flat roof: Loading characteristics and strategy of reduction. *Wind. Struct.* **2005**, *8*, 357–372. [[CrossRef](#)]
- Peng, H.; Dai, S.; Liu, H. Wind loading characteristics and roof zoning of solar arrays mounted on flat-roofed tall buildings. *J. Build. Eng.* **2023**, *66*, 105823. [[CrossRef](#)]
- Yang, Y.; Dong, L.; Li, J.; Li, W.; Sheng, D.; Zhang, H. A refined model of a typhoon near-surface wind field based on CFD. *Nat. Hazards* **2022**, *114*, 389–404. [[CrossRef](#)]
- Ren, H.; Laima, S.; Chen, W.L.; Zhang, B.; Guo, A.; Li, H. Numerical simulation and prediction of spatial wind field under complex terrain. *J. Wind. Eng. Ind. Aerodyn.* **2018**, *180*, 49–65. [[CrossRef](#)]
- Zhong, M.; Huang, B.; Li, Z.; Zhou, Z.; Liu, Z. Study on Probabilistic Properties of Fluctuating Wind Pressure Distribution of Low-Rise Buildings Affected by Slope Gradient in Mountain Forms. *Symmetry* **2022**, *14*, 2513. [[CrossRef](#)]
- Zhang, M.; Yu, J.; Zhang, J.; Wu, L.; Li, Y. Study on the wind-field characteristics over a bridge site due to the shielding effects of mountains in a deep gorge via numerical simulation. *Adv. Struct. Eng.* **2019**, *22*, 3055–3065.
- Ren, L.; Zeng, J.; Zeng, S. Wind Load of Kulangsu Historical and Cultural District Effected by Hilly Terrain. *Mt. Res.* **2019**, *37*, 41–52.
- Zhou, R.; He, X. Numerical simulation and character analysis of wind field in complex terrain in Hami Xinjiang. *Plateau Meteorol.* **2018**, *37*, 1413–1427.
- Wang, J.; Ding, W.; Wu, Y. Wind tunnel test of wind pressure distribution on mutual insert multi-greenhouse roof. *Trans. Chin. Soc. Agric. Eng.* **2008**, *24*, 230–234.
- Yang, Z.; Zhang, B.; Xue, X.; Huang, C.; Zhu, K. The wind tunnel test of plastic greenhouse and its surface wind pressure patterns. *Acta Ecol. Sin.* **2012**, *32*, 7730–7737. [[CrossRef](#)]
- Moriyama, H.; Sase, S.; Uematsu, Y.; Yamaguchi, T. Wind tunnel study of the interaction of two or three side-by-side pipe-framed greenhouses on wind pressure coefficients. *Trans. ASABE* **2010**, *53*, 585–592. [[CrossRef](#)]
- Kwon, K.S.; Kim, D.W.; Kim, R.W.; Ha, T.; Lee, I.B. Evaluation of wind pressure coefficients of single-span greenhouses built on reclaimed coastal land using a large-sized wind tunnel. *Biosyst. Eng.* **2016**, *141*, 58–81. [[CrossRef](#)]
- Li, Z.; Wei, Q.; Sun, Y. Experimental research on amplitude characteristics of complex hilly terrain wind field. *Eng. Mech.* **2012**, *29*, 184–191.

24. Zhou, D. The Study of Complex Hilly Terrain's Influence on Wind Loads Prediction of High-Rise Buildings. Master's Thesis, Chongqing University, Chongqing, China, 2015.
25. Xie, X.; Chen, K. Simulation test of wind load characteristics of south China type single-span plastic greenhouse. *Trans. Chin. Soc. Agric. Eng.* **2000**, *16*, 90–94.
26. Hoxey, R.P.; Robertson, A.P.; Basara, B.; Younis, B.A. Geometric parameters that affect wind loads on low-rise buildings: Full-scale and CFD experiments. *J. Wind. Eng. Ind. Aerodyn.* **1993**, *50*, 243–252. [[CrossRef](#)]
27. Mathews, E.H.; Meyer, J.P. Numerical modelling of wind loading on a film clad greenhouse. *Build. Environ.* **1987**, *22*, 129–134. [[CrossRef](#)]
28. Mathews, E.H.; Crosby, C.P.; Visser, J.A.; Meyer, J.P. Numerical prediction of wind loads on buildings. *J. Wind. Eng. Ind. Aerodyn.* **1988**, *31*, 241–250. [[CrossRef](#)]
29. Mathews, E.H.; Meyer, J.P. Computation of wind loads on a semicircular greenhouse. *J. Wind. Eng. Ind. Aerodyn.* **1988**, *29*, 225–233. [[CrossRef](#)]
30. Abdullah, J.; Zaini, S.S.; Aziz, M.A.; Majid, T.A.; Deraman, S.N.C.; Yahya, W.N.W. CFD prediction on the pressure distribution and streamlines around an isolated single-story house considering the effect of topographic characteristics. *IOP Conf. Ser. Earth Environ. Sci.* **2018**, *140*, 012006. [[CrossRef](#)]
31. Yao, J.F.; Shen, G.H.; Yao, D.; Xing, Y.L.; Lou, W.J. CFD-based numerical simulation of wind field characteristics on valley and col terrain. *J. Harbin Inst. Technol.* **2016**, *48*, 165–171.
32. Fernández-García, M.S.; Vidal-López, P.; Rodríguez-Robles, D.; Villar-García, J.R.; Agujetas, R. Numerical simulation of multi-span greenhouse structures. *Agriculture* **2020**, *10*, 499. [[CrossRef](#)]
33. Zhang, J.; Zhu, H. Analysis of wind vibration response of transmission wire fluid-structure coupling under canyon topography. *Chin. J. Appl. Mech.* **2021**, *38*, 693–699.
34. Tao, Y.; Lv, J.; Qiao, K.; Yuan, J. Numerical simulative research on Venlo-type greenhouse wind load character. *J. Agric. Mech. Res.* **2014**, *36*, 45–48.
35. Lv, J. The Numerical Simulation Research on Wind Load Characteristics of the Typical Greenhouse. Master's Thesis, Southwest University, Chongqing, China, 2013.
36. Wu, K.; Wang, S.J.; Zhang, G.P.; Wei, M.; Liu, F.S.; Lü, X. Wind-induced interference effects and wind pressure characteristics of arched plastic greenhouses. *Trans. Chin. Soc. Agric. Eng.* **2019**, *35*, 165–174.
37. Yan, F.; Li, W. On wind pressure on greenhouses with a pointed roof with numerical simulation. *J. Southwest China Norm. Univ. (Nat. Sci. Ed.)* **2017**, *42*, 127–132.
38. Liang, Z.; He, G.; Li, Y.; Gao, Z.; Ren, X.; Wu, Q.; Zhao, S.; Xu, J. Analysis of Wind Pressure Coefficients for Single-Span Arched Plastic Greenhouses Located in a Valley Region Using CFD. *Agronomy* **2023**, *13*, 553. [[CrossRef](#)]
39. Xu, J.; He, G.; Ren, X.; Hu, Z. Research on wind pressure distribution of plastic greenhouses in valley topography. *Eng. Agric.* **2022**, *42*, e20220075. [[CrossRef](#)]
40. Wang, J.; Ding, W. Simulation of wind pressure distribution on mutual insert multi-greenhouse. *Trans. Chin. Soc. Agric. Mach.* **2007**, *38*, 90–93.
41. Wang, J.; Wang, X.; Ding, W. ANSYS CFD simulation of airflow distribution in a tunnel greenhouse under wind driven situation. *Trans. Chin. Soc. Agric. Mach.* **2007**, *38*, 114–117.
42. Huang, B.; Wang, C. *Principle and Application of Structural Wind Resistance Analysis*; Tongji University Press: Shanghai, China, 2008.
43. Zhang, C.; Ren, S.; Yang, P.; Zhang, Z.; Guo, M. Research on the CFD simulation accuracy of labyrinth path drip irrigation cylindrical emitter. *J. China Agric. Univ.* **2016**, *21*, 149–155.
44. Zheng, J.; Zhang, Y.; Dou, Y. Study on the effect of turbulence model on the flow and heat transfer in the meandering channel based on the principle of high efficiency and energy saving. *Fresenius Environ. Bull.* **2020**, *29*, 2547–2554.
45. Zhang, B. Investigation into Brush Seal Internal Flow and Heat Transfer Based on Micro Tube Bank Models. Master's Thesis, Kunming University of Science and Technology, Kunming, China, 2012.
46. He, G. Study on the Influence of Valley Topography on the Wind Pressure Distribution Coefficient of Plastic Greenhouses. Master's Thesis, China Agricultural University, Beijing, China, 2022.
47. Murakami, S.; Mochida, A. 3-D numerical simulation of airflow around a cubic model by means of the  $k$ -model. *J. Wind. Eng. Ind. Aerodyn.* **1988**, *31*, 283–303. [[CrossRef](#)]
48. Richards, P.J.; Hoxey, R.P. Pressures on a cubic building—Part 1: Full-scale results. *J. Wind. Eng. Ind. Aerodyn.* **2012**, *102*, 72–86. [[CrossRef](#)]

**Disclaimer/Publisher's Note:** The statements, opinions and data contained in all publications are solely those of the individual author(s) and contributor(s) and not of MDPI and/or the editor(s). MDPI and/or the editor(s) disclaim responsibility for any injury to people or property resulting from any ideas, methods, instructions or products referred to in the content.